DOI:10.28974/idojaras.2024.4.2

IDŐJÁRÁS

Quarterly Journal of the HungaroMet Hungarian Meteorological Service
Vol. 128, No. 4, October – December, 2024, pp. 425–438

Investigation of 15 knots tailwind triggering go-around maneuver of eight flights at the Soekarno-Hatta International Airport using the WRF-ARW model

Achmad F. Rais [1,*], **Heri Ismanto** [2], **Eko Widyantoro** [3], **Bayu Umbaran** [2], and **Rezky Yunita**[4]

[1]*Research and Innovation Agency of Indonesia (BRIN), Bogor*

[2]*Center for Aeronautical Meteorology (BMKG), Jakarta*

[3]*Meteorological Station of Soekarno Hatta International Airport (BMKG), Tangerang*

[4]*Center for Research and Development (BMKG), Jakarta*

**Corresponding Author E-mail: achm050@brin.go.id*

(Manuscript received in final form January 3, 2024)

Abstract— A numerical simulation of the 15 knots tailwind triggering the go-around maneuver of 8 flights at the Soekarno-Hatta International Airport was explored. The Advancer Weather Research an Forecasting (WRF-ARW) numerical weather prediction model was used to simulate the events. The results showed that WRF-ARW with temporal and spatial resolutions of 2 minutes and 1 km could simulate the tailwind events. The tailwind was triggered by the background wind from the Indian Ocean and by cloud initiation near the final approach path (FAP), then the tailwind speed was reduced by the wind gust south of the FAP at 11:00 UTC, on November 3, 2021. These findings cannot be resolved by analyzing in-situ, weather satellite, and radar data with limited coverage and sensing the wind out of the cloud. It suggests that high-resolution numerical simulation can be used in the operation of aviation weather investigation. Assimilating observation data to the model is essential to be investigated for further study to understand the tailwind mechanism more accurately.

Key-words: background wind, downburst, airplane trajectory, final approach path.

1. Introduction

Airplane accidents related to weather primarily stem from dynamic factors, with wind being a significant contributor (*Gultepe et al.*, 2019). Wind is defined as the movement of air in any direction (*Ahrens* and *Henson*, 2014; *Stull*, 2020), and its assessment necessitates the utilization of both on-site and remote sensing technologies to provide quantitative measurements at surface and upper air levels (*WMO*, 2021; *Arta Kusuma et al.*, 2022). Data from these sources enables meteorologists to evaluate wind conditions for aviation safety accurately. The wind generation is attributed to a combination of forces, including the pressure gradient force, gravity, Coriolis force, centrifugal force, and friction (*Oliver*, 2005).

A flight's approach and landing phases account for more than half of all fatal accidents (*Boeing*, 2021). To address this, the go-around maneuver is employed, which involves discontinuing the approach or landing, and instead, initiating another attempt or diverting to alternate airports. The implementation of this procedure has proven to be effective in preventing 54% of potential accidents. Additionally, permissible crosswind components, as the Federal Aviation Administration (FAA) and the International Civil Aviation Organization (ICAO) stipulated, range from 10 to 20 knots (19 to 37 kilometers per hour), depending on runway dimensions and the airport reference code (*Chang*, 2015). Tailwinds can lead to accidents when they exceed speeds of 10 knots (*Blajev*, 2017). Depending on the aircraft type, the minimum tailwind value for a go-around is generally set at 10 knots (*Es* and *Karwal*, 2001). A tailwind is a wind blowing in the same direction as an airplane's flight path. Tailwinds are calculated based on the projection of wind direction onto the direction of the runway in use (*Rais et al.*, 2020), providing additional thrust during the landing phase.

On November 3, 2021, the pilots executed a go-around maneuver for eight aircrafts in the process of approaching the runway at the Soekarno-Hatta International Airport. The pilots reported encountering a 15-knot tailwind near runways 07 right (07R) and 07 left (07L) within a brief timeframe from 09:58 to 10:12 UTC. The presence of this tailwind can have an impact on aircraft operations at the Soekarno-Hatta International Airport. Given the extensive volume of over two million domestic flights and aircraft movements in 2018, the potential risks associated with such winds should not be underestimated (*PUSTIKOM*, 2019).

Numerical weather prediction (NWP) has proven to be a valuable instrument in investigating aviation incidents, allowing researchers to probe meteorological factors in regions and altitudes devoid of direct observations. In a study by *Regmi et al*. (2020), 13 plane accidents in Nepal attributed to near-surface turbulence were researched utilizing NWP. *Verayanti* and *Kusuma* (2021) and *Andari et al.* (2022) used NWP simulations to identify turbulence in the vicinity of clouds, which contributed to the turbulent flight paths of aircraft ID6890 on October 24, 2017, and EY474 on May 4, 2016. *Chan* (2014) also focused on forecasting

tailwinds resulting from wind interaction with terrain via NWP simulations. *Tse et al.* (2014) showcased NWP's capability to predict tailwinds associated with thunderstorms. Meanwhile, *Sardjono et al.* (2021) simulated tailwinds with the weather research and forecasting (WRF) model that closely matched observations.

The analysis of tailwinds during the approach phase at various altitudes using NWP has been a relatively underexplored area of research. *Chan* (2014) and *Tse et al.* (2014) conducted some of these limited studies. Most of the existing research primarily relies on surface wind data (*Fadholi*, 2013; *Perdana* and *Putra*, 2017; *Nanda et al.*, 2020; *Sardjono et al.*, 2021), sometimes in combination with satellite imagery and 1000 feet (305 meters) wind data to investigate the atmospheric dynamics during tailwinds (*Rais et al.*, 2020). To further delve into this phenomenon, we intend to employ the Weather Research and Forecasting (WRF) model to comprehensively analyze the mechanisms that induce tailwinds and enhance our comprehension of the underlying atmospheric processes.

2. Materials and method

We analyzed go-around reports from four aircrafts over runway 07L, namely JT023, GA221, QG251, and QG331, and four aircrafts over runway 07R, namely JT291, ID6871, GA113, and JT335. These reports highlight go-around actions due to 15-knot tailwinds during approaches at the Soekarno-Hatta International Airport on November 3, 2021. These reports were sourced from the air navigation services provider AirNav Indonesia, and we cross-referenced them with aircraft trajectories obtained from flightradar24 for confirmation. The details of these go-around incidents are provided in *Table 1*.

Table 1. AirNav Reports of the Go-around

Aircraft	Go-around	Landing
JT023	09:58UTC RWY 07L	10:28 UTC RWY 25R
JT291	10:05UTC RWY 07R	10:30 UTC RWY 25L
GA221	10:06UTC RWY 07L	10:30 UTC RWY 25R
ID6871	10:07UTC RWY 07R	10:33 UTC RWY 25L
QG251	10:08UTC RWY 07L	10:40 UTC RWY 25R
GA113	10:09UTC RWY 07R	10:36 UTC RWY 25L
QG331	10:12UTC RWY 07L	10:35 UTC RWY 25R
JT355	10:11UTC RWY 07R	10:39 UTC RWY 25L

We employed the Advanced Research Weather Research and Forecasting (ARW-WRF) version 4.1 numerical weather prediction model (*Skamarock et al.*, 2019). The WRF-ARW model is widely used in aviation meteorological analysis. *Chan* (2014), *Tse et al*. (2014), *Regmi et al*.(2020), *Verayanti* and *Kusuma* (2021), *Sardjono et al*. (2021), and *Andari et al*. (2022) use the WRF-ARW in their research. For the initial conditions, we utilized data from the NCEP GDAS/FNL (Global Data Assimilation System/Final Analysis of the National Centers for Environmental Prediction, USA) with a horizontal grid resolution of 0.25° and a temporal resolution of 6 hours, covering the period from November 2, 2021, 18 UTC to November 3, 2021, 12 UTC. The WRF-ARW configuration is detailed in *Table 2*. To validate the cloud top temperature of the WRF-ARW model, we used satellite observation data of the Himawari 8 geostationary meteorological satellite operated by the Japan Meteorological Agency and computed the correlation coefficient between 09:50 and 11:00 UTC. Further information regarding the model configuration can be found in *Table 2*. *Fig. 1* presents the three models domains (D1, D2, and D3) used for simulations by the WRF-ARW model.

Table 2. WRF-ARW configuration for domain 1 (D1), domain 2 (D2), and domain 3 (D3)

	D1	**D2**	**D3**
Resolution	9 km	3 km	1 km
Temporal interval	3 hours	1 hour	2 minutes
Vertical Layer	34	34	34
Parameterization	Tropical	Tropical, Cu=0	Tropical, Cu=0
Topography	GMTED	GMTED	SRTM 1s

We employed tropical-specific physical parameterizations, which included the WRF single moment 6 class (WSM6) scheme for microphysics, the newer Tiedtke scheme for cumulus convection, the rapid radiation transfer model for global circulation models (RRTMG) scheme for shortwave and longwave radiations, and the Yonsei University scheme for the boundary layer. Notably, the WSM6 scheme encompasses graupel production within the microphysical processes (*Song-You Hong* and *Jeong-Ock Jade Lim*, 2006), a feature that distinguishes it from WSM5 *(Lim* and *Hong 2005)*. The newer Tiedtke scheme calculates mixing ratios for cloud and ice, momentum tendencies, and shallow convection (*Skamarock et al.*, 2019). This scheme has demonstrated the ability to capture the fundamental characteristics of the marine boundary layer structure and low clouds (*Zhang et al.*, 2011), as well as to offer improved diurnal precipitation simulation (*Sun and Bi*, 2019). Additionally, the RRTMG scheme delivers radiative forcing results that exhibit closer agreement with high-resolution calculations (*Iacono et al.*, 2008).

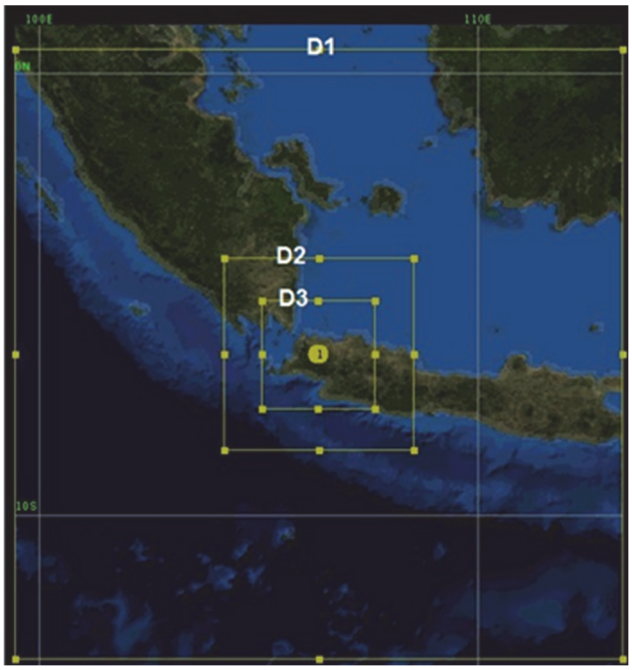

Fig. 1. WRF-ARW domain 1 (D1), domain 2 (D2), and domain 3 (D3).

The following equation was used to calculate the tailwind based on vector projection to the runway in use (*Belo-Pereira*, 2015; *Maruhashi et al.,* 2019; *Rais et al.*, 2020) :

$$Tw = -f\cos(d - r), \tag{1}$$

where *Tw* is the tailwind (kt), *f* is the wind speed (kt), *d* is the wind direction (°), and *r* is the direction of the runway in use (°).

3. Results and discussion

3.1. Track analysis

Fig. 2 shows that aircraft destined for runway 07L follow a relatively shorter final approach path (FAP), denoted as A-B compared to the trajectories leading to runway 07R, marked as C-D. A-B and C-D measure 9.15 nautical miles (approximately 16.94 kilometers) and 15 nautical miles (roughly 27.78 kilometers), respectively. It is worth noting that the maximum allowable FAP length, as per ICAO standards (*ICAO*, 2018), is 15 nautical miles. Aircraft flying over segment A transitioned from an altitude of 2175 feet to 2875 feet, while those over segment C experienced altitude changes from 4150 feet to 4225 feet. Moreover, runway 07 is more susceptible to tailwinds due to a higher incidence of wind blowing from the direction of runway 07 than runway 25, as indicated by windrose analysis (*Sardjono et al.*, 2021).

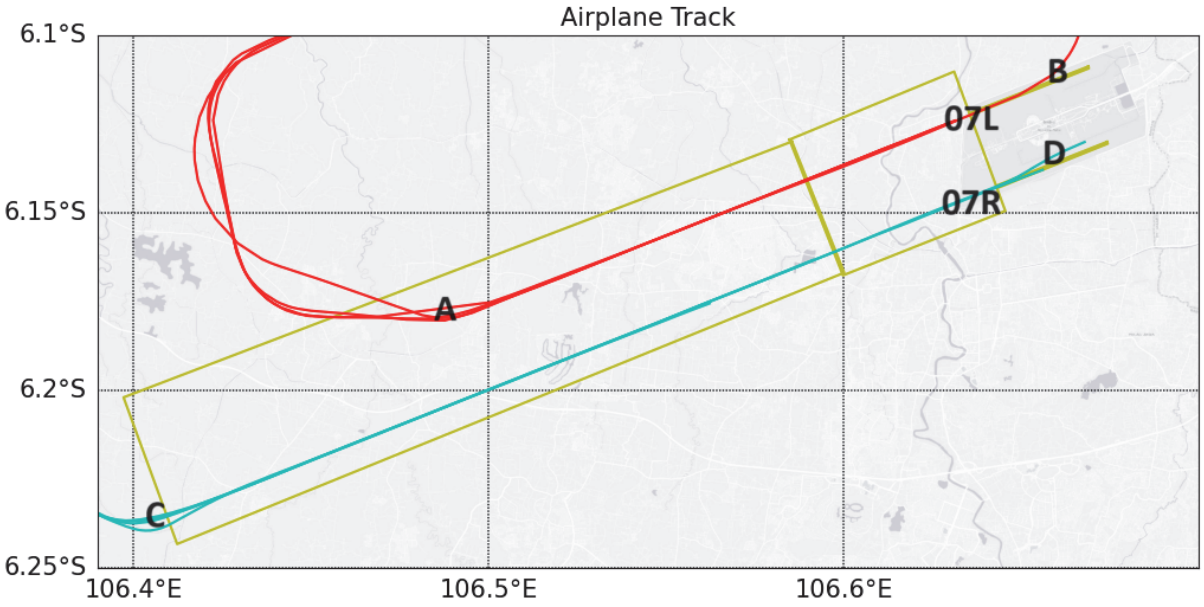

Fig. 2. Flights tracking to runway 07L (red line), runway 07R (cyan line), ARENA (small box), and FAP (small box + big box).

In sections A-B (*Fig. 3*), four flights, namely JT023, GA221, QG251, and Q331 traverse the A-B segment within specific time windows: 09:56 to 10:00, 10:04 to 10:08, 10:06 to 10:08, and 10:08 to 10:12, respectively. Among these aircraft JT023, GA221, and QG251 approach altitudes of 700 feet (213 meters), 500 feet (152 meters), and 450 feet (137 meters) above the surface, respectively, before executing a go-around maneuver and subsequently taking off again. These planes performed the go-around near the ARENA area, located at 3 nautical miles (5556 meters) from the runway, as indicated by *Chan* and *Hon* (2016).

Conversely, the QG331 aircraft maintains an approach altitude of only up to 1675 feet (510 meters). Notably, all aircraft experienced a consistent tailwind of approximately 15 knots (8 meters per second) at altitudes of up to 1500 feet (457 meters). This specific altitude represents the low-level wind shear region, where atmospheric dynamics significantly influence aircraft take-off and landing procedures, in accordance with ICAO guidelines (*ICAO*, 2005).

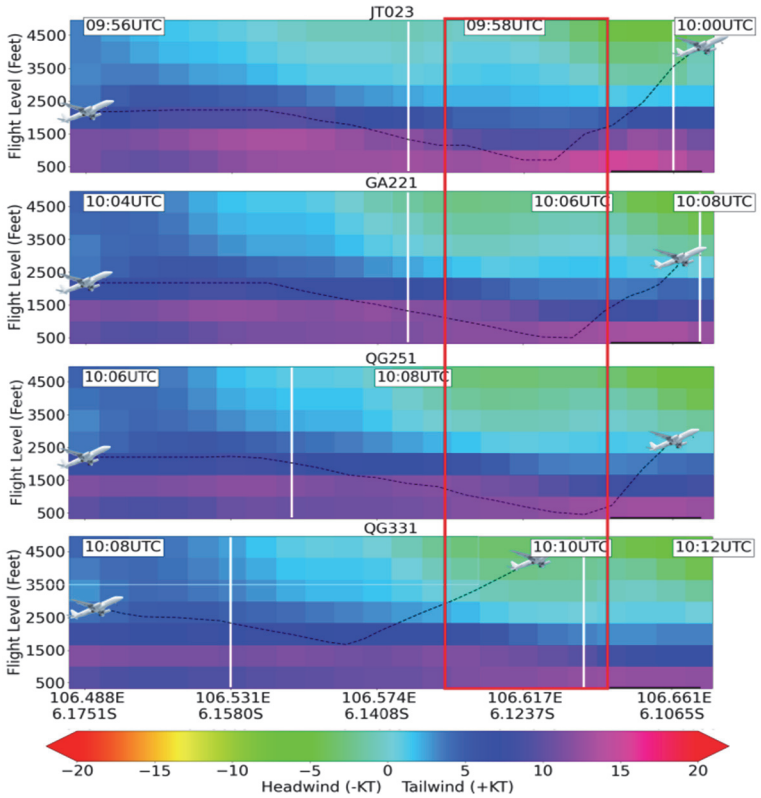

Fig. 3. Tailwind/Headwind (kt) in the A-B section overlayed by vertical flight track to runway 07L in every 2 minutes. The red box is ARENA, and the black line at the bottom right is the runway.

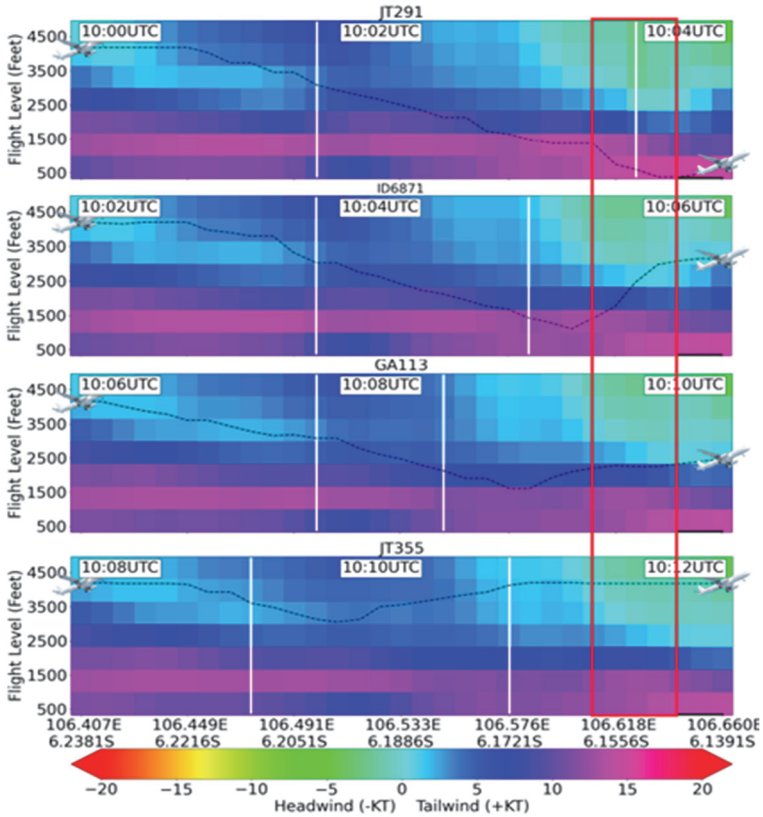

Fig. 4. Tailwind/Headwind (kt) in the C-D section overlayed by vertical flight track to runway 07L in every 2 minutes. The red box is ARENA, and the black line at the bottom right is the runway.

Within the C-D segment (*Fig. 4*), flights JT291, ID6871, GA113, and JT355 traverse the C-D portion during specific intervals: 10:00 to 10:04, 10:02 to 10:06, 10:06 to 10:10, and 10:08 to 10:12 UTC, respectively. The altitudes at which these aircrafts operate at the lowest points are 250 feet (76 meters) for JT291, 1100 feet (335 meters) for ID6871, 1600 feet (487 meters) for GA113, and 3050 feet (929 meters) for JT355. Of these, JT291 is in closest proximity to the runway.

As observed in the A-B sections, tailwinds persist at lower altitudes along the C-D route. These tailwinds, measured at 15 knots (8 m/s), surpass the minimum limit for B737 aircraft (10 knots or 5 m/s) and reach the tailwind limit for A320 aircraft, set at 15 knots or 8 m/s, as reported by *Es* and *Karwal* (2001). It is worth noting that the final approach path (FAP) to runway 07L experiences lower tailwind speeds than the FAP for runway 07R. Further exploration of this aspect will be undertaken in the Numerical Weather Prediction analysis section.

3.2. NWP analysis

This outcome validates the cloud top temperature of the WRF-ARW model, indicating a correlation coefficient of 0.6286 compared to the cloud top temperature of Himawari 8. This value closely resembles the correlation found in the study of *Chae* and *Sharewood* at an altitude of 14 km (*Chae* and *Sherwood*, 2010).

In *Fig. 5*, it is evident that a 15-knot (8 m/s) wind is present over the Indian Ocean, located to the south of Java, from 09:58 UTC to 10:12 UTC, at an altitude of 1500 feet (457 meters), and it shifts towards the final approach path (FAP). According to *Kurniawan et al*. (2011), wind speeds in this region, specifically the Indian Ocean, can reach up to 20 knots or 10 m/s during November. These strong winds result from the still-active Australian winter monsoon (*Alifdini*, 2021).

In area A, the wind entering the FAP is not obstructed by any terrain features, as indicated by the absence of white contours. As a result, the wind within the FAP region maintains a speed of 15 knots (8 m/s). Furthermore, the air mass located over the FAP is drawn into an area of wind convergence, denoted as area B. Wind convergence describes the phenomenon, where wind vectors converge towards a common point (*Stull*, 2020). This convergence of winds is closely associated with cloud formation, as *Banacos et al.* (2005) outlined.

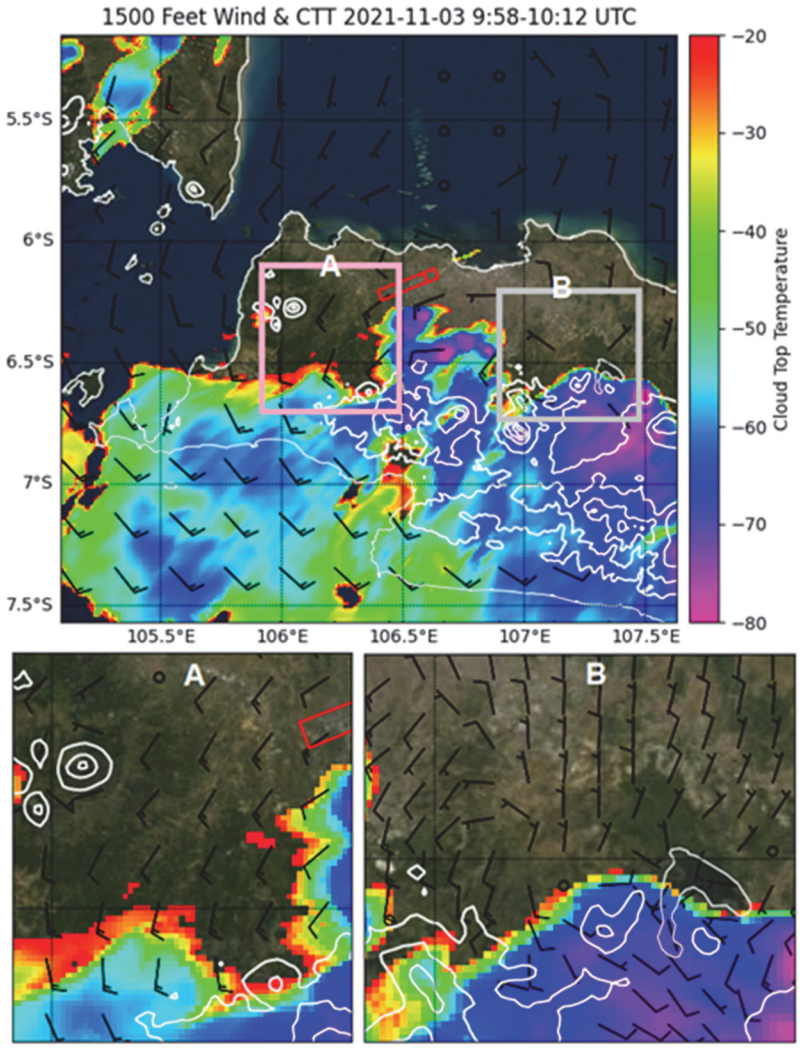

Fig. 5. Composite wind 1500 ft (457 m) over D3 from 09:58 to 10:12 UTC. The red box is the FAP. Box A and Box B are the areas of interest in the analysis.

The tailwind speed over the A-B segment is comparatively lower than the C-D segment (*Figs. 3* and *4*). This disparity is because the wind from the Indian Ocean initially reaches the C-D segment before progressing to A-B. As mentioned, C-D represents a longer trajectory than A-B, resulting in a broader wind coverage.

Fig. 6 shows a notable presence of vertical wind in area B, extending to an altitude of 20,000 meters (approximately 65,616 feet). This upward vertical movement of air masses at lower levels is significant. As *Shinozaki et al.* (2019) discussed, cloud analysis can be conducted based on cloud fraction. A higher cloud fraction indicates a greater cloud density. It is worth noting that at 09:59 UTC, convective clouds were still forming, reaching an altitude of 10,000 meters (around 32,808 feet). The convection in this area draws air masses from the Indian Ocean, causing a 15-knot wind to enter the FAP in a parallel direction.

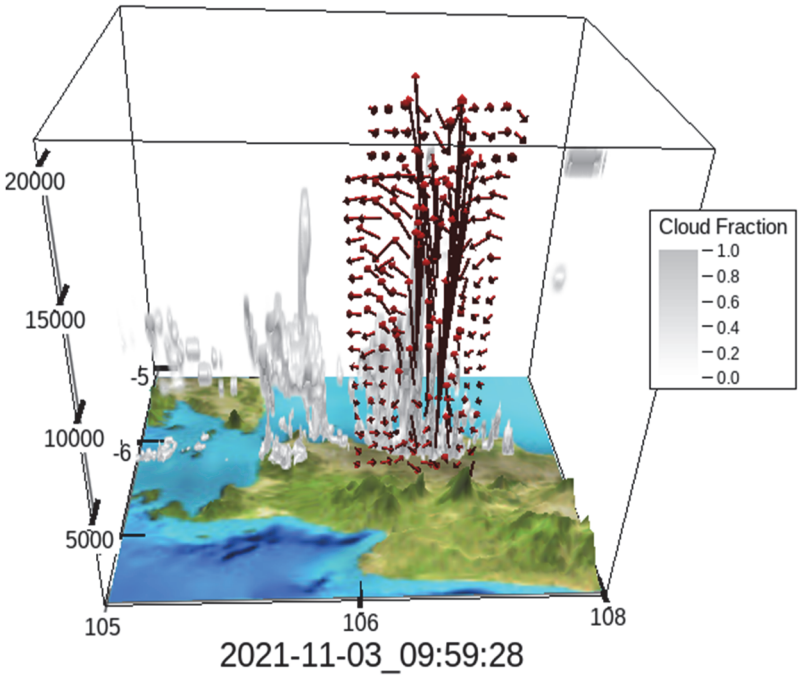

Fig. 6. A vertical section of wind in area B (*Fig. 5*) is overlayed with cloud fraction.

At 11 UTC (*Fig. 7*), a cloud with a cold top (around -80 °C), is observed south of the FAP. A cold top indicates a high cloud altitude. In area A, there is a presence of wind divergence. This divergence causes the wind, which previously flowed in the same direction as the FAP, to veer towards the north. This, in turn, influences the *d-r* component in Eq.(1), causing it to expand and reduce the cosine value. As a result, the tailwind magnitude becomes smaller.

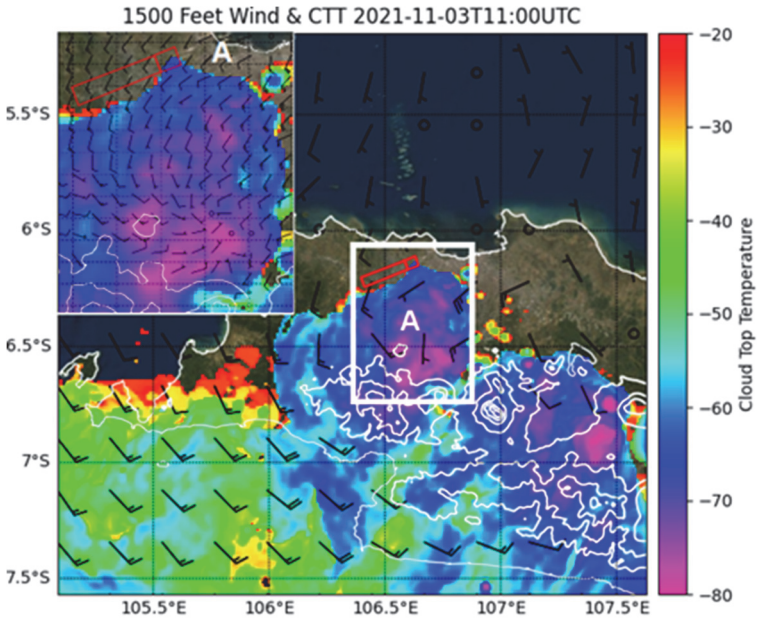

Fig. 7. Wind at 1500 ft (457 m) over D3 at 11:00 UTC. The red box is the FAP. Box A is the area of interest in the analysis.

Fig. 8 shows that high-altitude clouds with tops reaching 20,000 meters (65,616 feet) are present in area A. Concurrently, there is noticeable downdraft activity blown from this mature cloud at lower altitudes. This downdraft generates divergence at a height of 1500 feet, similar to the findings in Yoshino's study (*Yoshino,* 2019). It is worth noting that compared to the research conducted by *Auly et al.* (2018), the wind gust observed in this case is not a result of the downdraft itself. Instead, it is initiated by the background wind originating from the Indian Ocean, which experiences a reduction due to the downdraft's influence, particularly in a direction perpendicular to the wind gust.

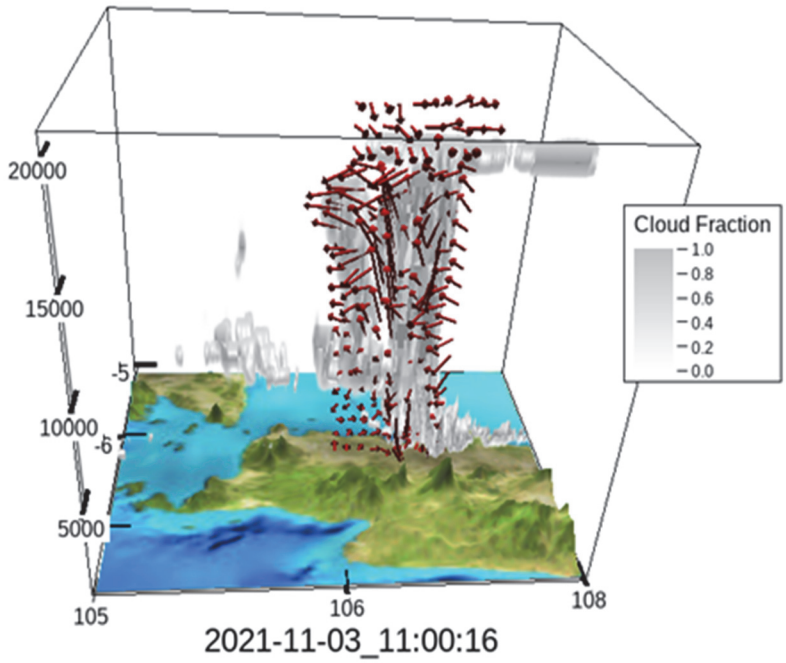

Fig. 8. A vertical section of wind over area A in *Fig. 7* is overlayed with cloud fraction.

4. Conclusions

We conducted weather simulations related to eight aircraft go-arounds to understand wind dynamics better. These simulations were performed using the WRF-ARW model with a spatial and temporal resolution of 1 km and 2 minutes, verified against Himawari 8 cloud top temperatures. Eight flights executed go-around maneuvers triggered by tailwinds, as depicted in *Figs. 3* and *4*, and these could be accurately simulated using WRF-ARW. In *Figs. 5* and *6*, we analyze that wind from the Indian Ocean, in conjunction with the cloud formation process, generated tailwinds over the FAP. Meanwhile, at 11:00 UTC, as evident in *Figs. 7* and *8*, we documented a reduction in wind speed due to gusts originating from downdrafts southward near the FAP.

This study has revealed the significant impact of background winds on tailwinds, a factor not explicitly addressed in previous researches. By expanding our analysis beyond the airport's observation points and utilizing the WRF-ARW model, this research provides valuable insights into how background winds can influence the occurrence of tailwinds. This knowledge holds the potential to enhance aviation safety and operational efficiency. Future research must assimilate observation data into the NWP for more precise investigations.

Funding: The research was performed without external funding.

References

Ahrens, C.D. and *Henson, R.*, 2014: Meteorology today: an introduction to weather, climate, and the environment. Cengage, 662 p.

Alifdini, I., 2021: Seasonal distribution and variability of surface winds in the Indonesian seas using scatterometer and reanalysis data 1–19. *Int. J. Climatol. 41,* 4825–4843. https://doi.org/10.1002/joc.7101

Andari, B.R.T., Trilaksono, N.J., and *Munandar, M.A.*, 2022: A Numerical Study of Near Cloud Turbulence Encounters over Bangka Island On 4 May 2016. *Jurnal Meteorlogi Klimatologi dan Geofisika*, 65–72. https://doi.org/10.31172/jmg.v23i3.912

Arta Kusuma, L.K.N., Pratiwi, I., Ismanto, H., and *Fitrianto, M.A.*, 2022: Utilization of Doppler Weather Surveillance Radar for Wind-Shear Detection in Airport, In: Proceedings - 2022 8th International Conference on Science and Technology, ICST 2022. Institute of Electrical and Electronics Engineers Inc. https://doi.org/10.1109/ICST56971.2022.10136300

Auly, A., Nugraha, A., and *Trilaksono, N.J.*, 2018: Simulation of Wind Gust – Producing Thunderstorm Outflow over Mahakam Block Using WRF 020051. *Jurnal Ilmu Fisika | Universitas Aandalas 15(2)*,175–187. https://doi.org/10.1063/1.5047336

Banacos, P.C., Oceanic, N., and *Schultz, D.M.*, 2005: The Use of Moisture Flux Convergence in Forecasting Convective Initiation: Historical and Operational Perspectives. *Semantic Scholar* ID: 2927533. https://doi.org/10.1175/WAF858.1

Belo-Pereira, M., 2015: Comparison of in-flight aircraft icing algorithms based on ECMWF forecasts. *Meteorol. Appl. 22*, 705–715. https://doi.org/10.1002/met.1505

Blajev, T., 2017: Go-Around Decision-Making and Execution Project. Flight Safety Foundation. https://flightsafety.org/wp-content/uploads/2017/03/Go-around-study_final.pdf

Boeing, 2021: Statistical Summary of Commercial Jet Airplane Accidents.

Chae, J.H. and *Sherwood, S.C.*, 2010: Insights into Cloud-top height and Dynamics from the Seasonal cycle of cloud-top heights observed by MISR in the west Pacific region. *J. Atmos.Scie. 67*, 248–261. https://doi.org/10.1175/2009JAS3099.1

Chan, P.W., 2014: A tail strike event of an aircraft due to terrain-induced wind shear at the Hong Kong international airport. *Meteorol. Appl. 21*, 504–511. https://doi.org/10.1002/met.1303

Chan, P.W. and *Hon, K.K.*, 2016: Observation and Numerical Simulation of Terrain-Induced Windshear at the Hong Kong International Airport in a Planetary Boundary Layer without Temperature Inversions. *Adv. Meteorol. 1016*. https://doi.org/10.1155/2016/1454513

Chang, S.W., 2015: Crosswind-based optimization of multiple runway orientations. *J. Adv. Transport. 49*, 1–9. https://doi.org/10.1002/atr.1247

Es, G.V. and *Karwal, A.K.*, 2001: Safety aspects of tailwind operations Safety aspects of tailwind operations. NLR-TP-2001-003. https://skybrary.aero/sites/default/files/bookshelf/1148.pdf

Fadholi, A., 2013: Analisis Komponen Angin Landas Pacu (Runway) Bandara Depati Amir Pangkalpinang. *Statistika 13*, 45–53.

Gultepe, I., Sharman, R., Williams, P.D., Zhou, B., Ellrod, G., Minnis, P., Trier, S., Griffin, S., Yum, S.S., Gharabaghi, B., Feltz, W., Temimi, M., Pu, Z., Storer, L.N., Kneringer, P., Weston, M.J., Chuang, H. ya, Thobois, L., Dimri, A.P., Dietz, S.J., França, G.B., Almeida, M. V., and *Neto, F.L.A.*, 2019: A Review of High Impact Weather for Aviation Meteorology. *Pure Appl. Geophys. 176*, 1869–1921. https://doi.org/10.1007/s00024-019-02168-6

Iacono, M.J., Delamere, J.S., Mlawer, E.J., Shephard, M.W., Clough, S.A., and *Collins, W.D.*, 2008: Radiative forcing by long-lived greenhouse gases: Calculations with the AER radiative transfer models. *J. Geophys. Res. Atmos. 113*. https://doi.org/10.1029/2008JD009944

ICAO, 2005: Manual on Low-level Wind Shear. ICAO.

ICAO, 2018: Annex 10 to the Convention on International Civil Aviation : Aeronautical Telecommunications. ICAO.

Kurniawan, R., Habibie, M.N., and *Suratno, S.*, 2011: Variasi Bulanan Gelombang Laut Di Indonesia. *Jurnal Meteorologi dan Geofisika*, *12*, 221–232. https://doi.org/10.31172/jmg.v12i3.104

Lim J.O.J and *Hong S.Y.* 2005 : Effects of bulk ice microphysics on the simulated monsoonal precipitation over east Asia. *J Geophys Res Atmos. 110(24):1–16.* https://doi.org/10.1029/2005JD006166.

Maruhashi, J., Serrano, P., and *Bello Pereira, M.*, 2019: Analysis of Mountain Wave Effects on a Hard Landing Incident in Pico Aerodrome Using the AROME Model and Airborne Observations. *Atmosphere 10*(7), 350; https://doi.org/10.3390/atmos10070350

Nanda, R.F., Sobirin, and *Saraswati, R.*, 2020: Place exposure pattern toward landslide disaster due to heavy rainfall in Probolinggo District, East Java, In: IOP Conference Series: Earth and Environmental Science. Institute of Physics Publishing. https://doi.org/10.1088/1755-1315/481/1/012058

Oliver, J.E., 2005: Encyclopedia of world Climatology. Springer, Dordrecht, 874 p. https://doi.org/10.1007/1-4020-3266-8

Perdana, Y.H. and *Putra, I.D.G.A.*, 2017: Kejadian Crosswind di Landasan Pacu Bandara Supadio Pontianak Tahun 2016, In: Seminar Nasional Iptek Penerbangan Dan Antariksa XXI-2017. 0–5.

PUSTIKOM, 2019: Statistik Perhubungan Buku I 2018. Kementrian Perhubungan, 224 p.

Rais, A.F., Wijayanto, B., and *Meinovelia, E.*, 2020: Analisis Tailwind Penyebab Go-Around pada 38 Bandara di Indonesia dalam Periode Januari-Februari 2020. *Warta Penelitian Perhubungan*, *32*, 77–82. https://doi.org/10.25104/warlit.v32i2.1546

Regmi, G., Shrestha, S., Maharjan, S., Khadka, A.K., Regmi, R.P., and Kaphle, G.C., 2020: The Weather Hazards Associated with the US-Bangla Aircraft Accident at the Tribhuvan International Airport Nepal. *Weather Forecast. 35*, 1891–1912. https://doi.org/10.1175/WAF-D-19-0183.1

Sardjono, W., Zulkarnain, Kusnoputranto, H., Soesilo, T.E.B., Utama, D.N., and *Sudirwan, J.*, 2021: Study of runway crosswind and tailwind potential for airport sustainability: A study of Soekarno Hatta airport, Cengkareng, Indonesia, In: IOP Conference Series: Earth and Environmental Science. IOP Publishing Ltd. https://doi.org/10.1088/1755-1315/729/1/012012

Shinozaki, K., Monte, S., Ferrarese, S., Manfrin, M., Bertaina, M.E., Anzalone, A., Bisconti, F., Bruno, A., and *Diaz, A.*, 2019: Cloud distribution evaluated by the WRF model during the EUSO-SPB1 flight 05006, 1–6. https://doi.org/10.1051/epjconf/201921005006

Skamarock, W.C., Klemp, J.B., Dudhia, J., Gill, D.O., Liu, Z., Berner, J., Wang, W., Powers, J.G., Duda, M.G., Barker, D.M., and *Huang, X.-Y.*, 2019: A Description of the Advanced Research WRF Model Version 4. Boulder. doi:10.5065/1dfh-6p97

Song-You Hong, and *Jeong-Ock Jade Lim*, 2006: The WRF Single-Moment 6-Class Microphysics Scheme (WSM6). *J Korean Meteorl. Soc. 42*(2) 129–151.

Stull, R., 2020: Practical Meteorology: An Algebra-based Survey of Atmospheric Science Roland. The University of British Columbia, 944 p.

Sun, B.Y., and *Bi, X.Q.*, 2019: Validation for a tropical belt version of WRF: sensitivity tests on radiation and cumulus convection parameterizations. *Atmos. Ocean. Sci. Lett. 12*, 192–200. https://doi.org/10.1080/16742834.2019.1590118

Tse, S.M., Chan, P.W., and *Wong, W.K.*, 2014: A case study of missed approach of aircraft due to tailwind associated with thunderstorms. *Meteorol. App. 21*, 50–61. https://doi.org/10.1002/met.1296

Verayanti, N P.T and *Kusuma, I.K.N.A.*, 2021: Simulasi Numerik Mekanisme Turbulensi Dekat Awan Konvektif. *Jurnal Sains and Teknologi Modifikasi CuacaModifikasi Cuaca 22*, 25–33. https://doi.org/10.29122/jstmc.v22i1.4560

WMO, 2021: Guide to Instruments and Methods of Observation Volume I-Measurement of Meteorological Variables, 2021st ed. WMO, Geneva.

Yoshino, K., 2019: Low-level wind shear induced by horizontal roll vortices at Narita international airport, Japan. *J. Meteorol. Soc. Japan 97*, 403–421. https://doi.org/10.2151/jmsj.2019-023

Zhang, C., Wang, Y., and Hamilton, K., 2011: Improved representation of boundary layer clouds over the southeast pacific in ARW-WRF using a modified tiedtke cumulus parameterization scheme. *Month. Weather Rev. 139*, 3489–3513. https://doi.org/10.1175/MWR-D-10-05091.1